Journal of Alloys and Compounds 509 (2011) L145–L149

Contents lists available at ScienceDirect

Journal of Alloys and Compounds

journal homepage: www.elsevier.com/locate/jallcom

Letter

Investigation on microstructure characterizations and phase compositions of rapidly solidification/powder metallurgy Mg–6 wt.% Zn–5 wt.% Ce–1.5 wt.% Ca alloy

Tao Zhou[a,*], Hua Xia[a], Mingbo Yang[a], Zhiming Zhou[a], Kang Chen[a], Jianjun Hu[a], Zhenhua Chen[b]

[a] College of Material Science and Engineering, Chongqing University of Technology, Chongqing 400054, China
[b] College of Material Science and Engineering, Hunan University, Changsha 410082, China

ARTICLE INFO

Article history:
Received 4 November 2010
Received in revised form
14 December 2010
Accepted 16 December 2010
Available online 24 December 2010

Keywords:
Rapidly solidification/powder metallurgy
Mg–Zn–Ce–Ca alloy
Microstructure
Thermal property

ABSTRACT

Rapidly solidification/powder metallurgy (RS/PM) Mg–6Zn–5Ce–1.5Ca (wt.%) alloy in form of rods has been prepared by hot extrusion with RS powders, produced via atomizing the alloy melt and subsequent splat-quenching on the water-cooled copper twin-rollers. Microstructure characterizations and phase compositions of the alloy have been investigated. The results showed that the RS/PM Mg–6Zn–5Ce–1.5Ca alloy was the characteristics of very fine grains with the size ranging from 200 to 650 nm and was composed of α-Mg, $Mg_xZn_yCe_z$ phase with a few Ca (about 1 at.%) shortened as the $Mg_xZn_yCe_z$–(Ca) phase, and a small quantity of $Mg_{51}Zn_{20}$ phases. The melting point of the $Mg_xZn_yCe_z$–(Ca) phase in the alloy was a little higher than that of the $Mg_xZn_yCe_z$ phase in RS/PM Mg–6Zn–5Ce alloy, which may be due to the dissolving of Ca in it. Moreover, the atomic percentage ratio of Zn to Ce in the $Mg_xZn_yCe_z$–(Ca) phase around the grain boundary was close to 1.5.

1. Introduction

Magnesium alloys are becoming increasingly attractive for engineering applications because of their particularly low density, excellent damping capacity, good recycling capacity and machinability. Their superior specific stiffness and strength offer a broad range of technical applications, particularly in the electronics, aerospace and automotive industries [1–4]. As one of the precipitation strengthening alloys, the Mg–Zn alloy exhibits moderate strength, good plasticity and corrosion resistance. However, the Mg–Zn alloy is the characteristics of poor casting property, strength at high temperatures and creep resistance, so its applications are remarkably limited [5]. A common approach to design of high strength, creep resistant alloys involves production of alloy microstructures containing uniform fine-scale dispersions of thermal stable intermetallic precipitates and such microstructures can be developed for magnesium alloys by non-equilibrium processing, such as rapidly solidification (RS) [6]. Thus, RS can play an important role due to its advantages, such as homogeneity of refined microstructure, extended solid solubility and formation non-equilibrium phases [7].

It has been reported that the casting property and creep resistance of Mg–Zn alloy can be improved with the RE additions and the Mg–Zn–RE alloys exhibit the age-hardening behaviour [8]. The Zn and Ce together with Mg may form the stable intermetallic compound MgZnRE, which is beneficial to the enhanced thermal stability of the alloys [9]. In recent years, great deals of investigations have been focused on the phase diagrams, microstructures and phase constitutions of the Mg–Zn–RE based alloys, but the results are various due to the variety of RE content [10–17]. The new die-castable Mg–Zn–Al–Ca–RE alloys for high temperature applications [18] have been developed and creep properties of some investigated alloys are far superior to those of conventional heat resistant AE42 magnesium alloy by means of the combined addition of alkaline-earth and RE elements, which has been found to be beneficial to the improvement of mechanical properties in cast magnesium alloys at elevated temperatures [19]. Moreover, Jun et al. [20] suggested that tensile yield strength for the ZE41 casting alloy was enhanced with increasing Ca content at all temperatures up to 300 °C, caused by the refined α grains and higher thermal stability of the Mg_7Zn_3–(RE)–(Ca) eutectic phase. Thus, Ca is considered to be added to further improve the mechanical properties of the Mg–Zn–RE alloys at high temperatures. However, it is difficult to find a systematic research on rapidly solidification/powder metallurgy (RS/PM) and phase constitutions of the Mg–6Zn–5Ce–1.5Ca alloy, although a few were reported on cast Mg–Zn–RE–Ca alloys [20,21]. Accordingly, in the present study, a small amount of Ca was added into RS/PM Mg–6Zn–5Ce alloy, and microstructure characterizations and phase compositions of the RS/PM Mg–6Zn–5Ce–1.5Ca alloy were investigated.

* Corresponding author. Tel.: +86 023 65030023; fax: +86 023 65030023.
E-mail addresses: ztlw8118@yahoo.com.cn, zt19811118@sina.com (T. Zhou).

0925-8388/$ – see front matter © 2010 Elsevier B.V. All rights reserved.
doi:10.1016/j.jallcom.2010.12.133

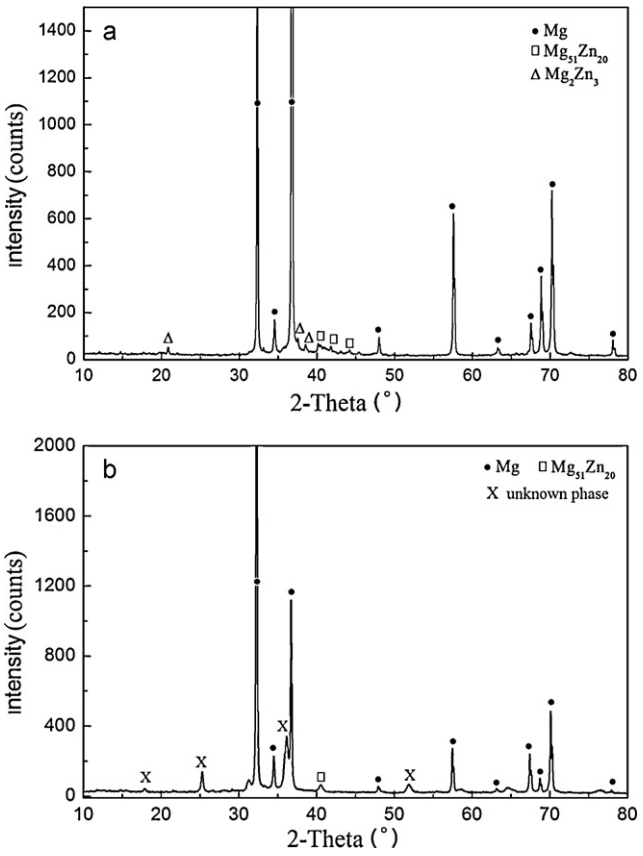

Fig. 1. X-ray diffraction pattern of the RS/PM Mg–Zn–X alloys: (a) Mg–6Zn and (b) Mg–6Zn–5Ce–1.5Ca.

2. Materials and methods

The material used in the present study was a RS/PM Mg–6Zn–5Ce–1.5Ca (wt.%) magnesium alloy. The RS/PM Mg–6Zn–5Ce–1.5Ca alloy was processed with RS powders, using pure (99.9%) magnesium, zinc, calcium, and cerium. The RS powders were produced by melting the alloys under the protection of Ar atmosphere in a steel crucible, atomizing the alloy melt and subsequent splat-quenching of the atomized drops on the water-cooled copper twin-rollers. Then the RS powders were hot-pressed at 300 °C in Ar atmosphere. The hot-pressed billets were extruded at 380 °C with a reduction ratio of 39:1.

Thermal property of the alloy was analyzed by differential scanning calorimetry (DSC, NETZSCH STA 449C), with the heating rate of 10 °C/min and under the protection of Ar atmosphere. Microstructural characterization of the alloy was carried out by X-ray diffraction (XRD, D8 Advance) using monochromatic Cu K_α radiation and transmission electron microscopy (TEM, Tecnai G220, 200 kV) at 200 kV. Thin foil specimens for TEM observation were twin-jet electropolished in a solution of 5.3 g lithium chloride, 11.6 g magnesium perchlorate, 500 ml methanol and 100 ml 2-butoxy-ethanol, at −55 °C and 85 V, and then by an ion beam milling.

3. Results

3.1. Phase constitutions

In order to study the phase compositions of the RS/PM Mg–6Zn–5Ce–1.5Ca alloy, the X-ray diffraction pattern of the RS/PM Mg–6Zn alloy was added, as seen in Fig. 1(a), because the quaternary alloy was formed on the basis of the Mg–6Zn alloy with Ce and Ca additions. It can be seen that the main peaks for the RS/PM Mg–6Zn alloy were corresponding to α-Mg, and small quantities of $Mg_{51}Zn_{20}$ and Mg_2Zn_3 phases. The XRD pattern of the RS/PM Mg–6Zn–5Ce–1.5Ca alloy is shown in Fig. 1(b). The main peaks for the alloy were corresponding to α-Mg, and small quantities of $Mg_{51}Zn_{20}$ phases as well as many unknown diffraction peaks were detected in the alloy as shown in Fig. 1(b) marked as X.

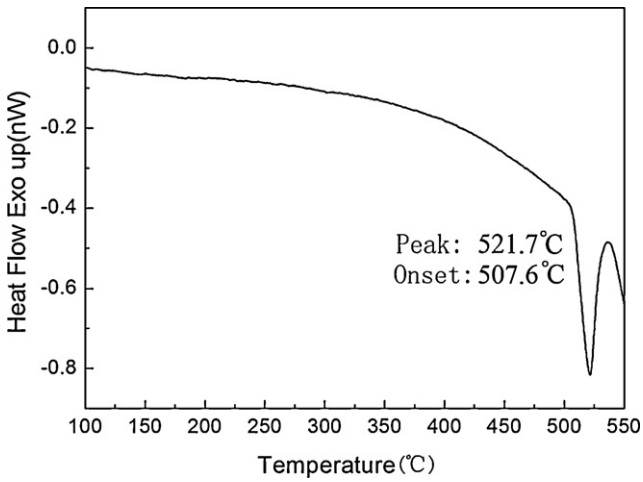

Fig. 2. DSC curve of the RS/PM Mg–6Zn–5Ce–1.5Ca alloy during heating.

3.2. Thermal property

The phase stability of the RS/PM Mg–6Zn–5Ce–1.5Ca was investigated by DSC. The heating curves from 100 to 550 °C with a rate of 10 °C/min are shown in Fig. 2. According to the results of previous study [22], RS/PM Mg–6Zn–5Ce alloy exhibited a large endothermic peak at 518.4 °C and the onset peak was 502.2 °C during heating. As the addition of 1.5 wt.% Ca to the Mg–6Zn–5Ce alloy (Fig. 2), the endothermic peak occurred at about 521.7 °C and the onset peak was 507.6 °C, a little higher than that of the former one.

3.3. Microstructure characterization

In order to understand the main reason for the endothermic peak existed in the DSC curve and the unknown peaks in the XRD of the RS/PM Mg–6Zn–5Ce–1.5Ca alloy, the detailed microstructure of the alloy was investigated by TEM/EDS. The microstructures of the RS/PM Mg–6Zn–5Ce–1.5Ca alloy are shown in Fig. 3. It can be seen that the maximum and minimum grain sizes of the alloy were approximately 650 nm and 200 nm, respectively. So the grain size of the alloy was about in the range of 200–650 nm, which was estimated directly from the TEM micrograph (Fig. 3(a)). A large number of precipitates with relatively larger size and a few fine precipitates were distributed at the grain boundary and in the grain interior, respectively (Fig. 3(a)). Another feature observed in the alloy was that many dislocations were observed around the precipitates (Fig. 3(b)) as marked by arrow. The local freezing time of the alloy was extremely limited due to the effect of RS, so a high vacancy density was formed in the RS flakes. Moreover, a large thermal stress existed in the alloy during the RS leaded to the accumulation and dilapidation of vacancies and then formation of many dislocations loops. Thus, a high vacancy density and dislocation density occurred in the RS alloy [23]. During the hot extrusion of the RS flakes, the supersaturated solid solution decomposed and the particles were firstly precipitated around the place with a high density of dislocations. In addition, the extrusion process could also lead to dislocation multiplication [24,25]. Thus, a relatively high dislocation density was detected around the precipitates in the alloy.

As seen from Fig. 4(a), a few cubic particles with relatively larger sizes were observed at the grain boundary as marked by arrows. The size of the cubic particles was approximately in the range of 350–640 nm in length and 200–460 nm in width, respectively. Analyzed by the EDS result of one of them (Fig. 4(b) marked as P), the Mg, Zn and Ce elements were concentrated in the particle, whereas a small quantity of Ca elements were also detected. Its composition

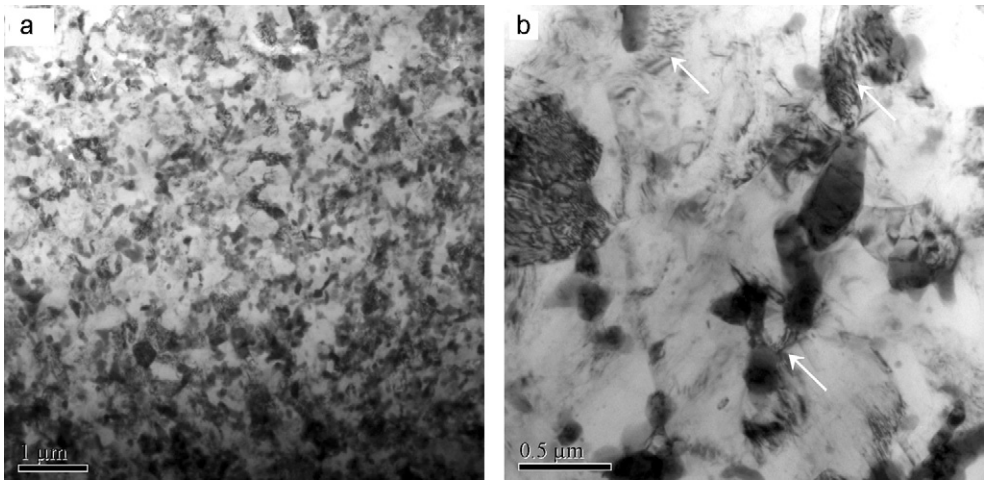

Fig. 3. TEM micrograph of the RS/PM Mg–6Zn–5Ce–1.5Ca alloy: (a) matrix and precipitates and (b) dislocations around the precipitates.

(wt.%) was 37.7 wt.% Mg, 24.8 wt.% Zn, 36.8 wt.% Ce and 0.8 wt.% Ca, corresponding to the atomic composition 70.1 at.% Mg, 17.1 at.% Zn, 11.9 at.% Ce and 0.9 at.% Ca, in which the atomic percentage ratio of Zn to Ce is close to 1.5 and the atomic percentage of Ca is about 1 at.%.

As seen from Fig. 5, many precipitates with different morphologies were also observed around the grain boundary. It could be seen that the precipitates were mostly cubic (Fig. 5(a)), strip (Fig. 5(a)) and near-spherical (Fig. 5(b)) in the alloy. One of the cubic precipitates with a relatively smaller size (marked as 5), strip (marked as 2) and near-spherical precipitates (marked as 4) was approximately 198 nm in length and 136 nm in width, 454 nm in length and 149 nm in width, and 142 nm in diameter, respectively. The corresponding EDS results (Fig. 5(c) and (d) and Table 1) of the precipitates and matrix (marked as 3 in Fig. 5(a)) indicated that the precipitates exhibited a pronounced enrichment of Mg, Zn and Ce elements, whereas a small quantity of Ca elements was also detected. As mentioned above, for the precipitates with different morphologies, the atomic percentage ratio of Zn to Ce was close to 1.5 and the atomic percentage of Ca was about 1 at.%.

Thus, it could be inferred that the $Mg_xZn_yCe_z$ phase with a few Ca (about 1 at.%) may be formed in the RS/PM Mg–6Zn–5Ce–1.5Ca alloy, the detailed discussion can be seen in Section 4.

4. Discussion

Based on the results of XRD, DSC and TEM with EDS, it can be confirmed that the $Mg_xZn_yCe_z$ phase with a few Ca (about 1 at.%) exist in the RS/PM Mg–6Zn–5Ce–1.5Ca alloy, which is similar to the results of literatures [20,21]. The detailed analysis is as follows: firstly, many unknown diffraction peaks can be observed in the alloys as seen from XRD (Fig. 1). Secondly, through the TEM and EDS analysis, there are many precipitates exhibited a pronounced enrichment of the Mg, Zn and Ce elements in the alloy, whereas a small quantity of Ca elements (about 1 at.%) are also detected in the precipitates, which is different from that of the T phase in Mg–Zn–RE alloys [14,26]. It was reported that there were three intergranular compounds in the as-cast and as-aged Mg–Zn–RE alloys and the mostly intergranular compounds were T phases with high RE contents [14]. Thirdly, Wei et al. [14] suggested that the formation temperature of T phase was at the range of 480–447 °C during the solidification of Mg–8Zn–1.5MM (wt.%) alloy. However, the formation temperature of T phase in Mg–10MM–5Zn (wt.%) alloy was about at the range of 585–500 °C much higher than that in the Mg–8Zn–1.5MM alloy [27]. According to the DSC result of the RS/PM Mg–6Zn–5Ce–1.5Ca alloy (Fig. 2), the onset temperature of the endothermic peak of the alloy is about 507 °C, closed to the for-

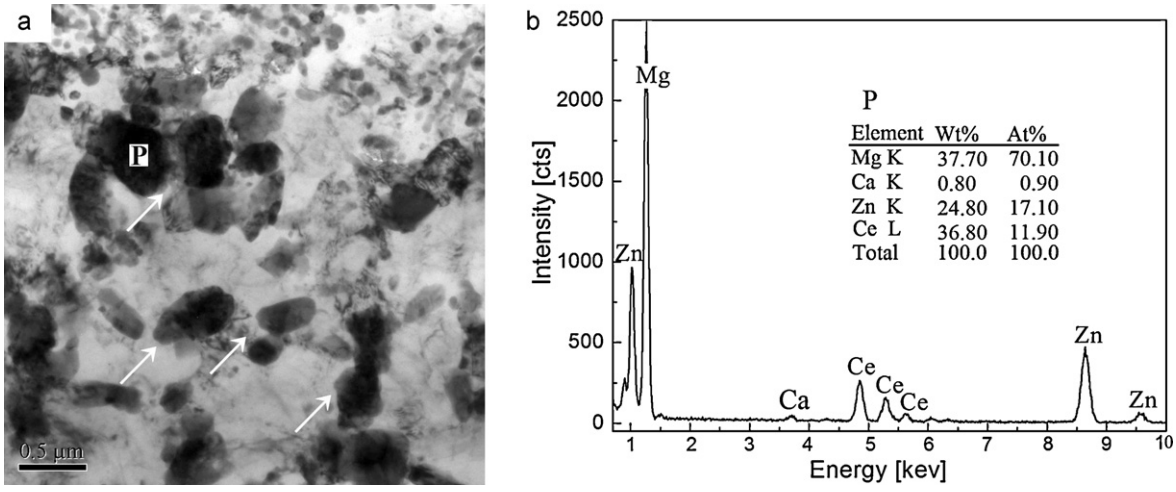

Fig. 4. TEM images of a few cubic particles with relatively larger sizes around the grain boundary in the alloy: (a) the image of matrix and precipitates and (b) EDS result of one particle P.

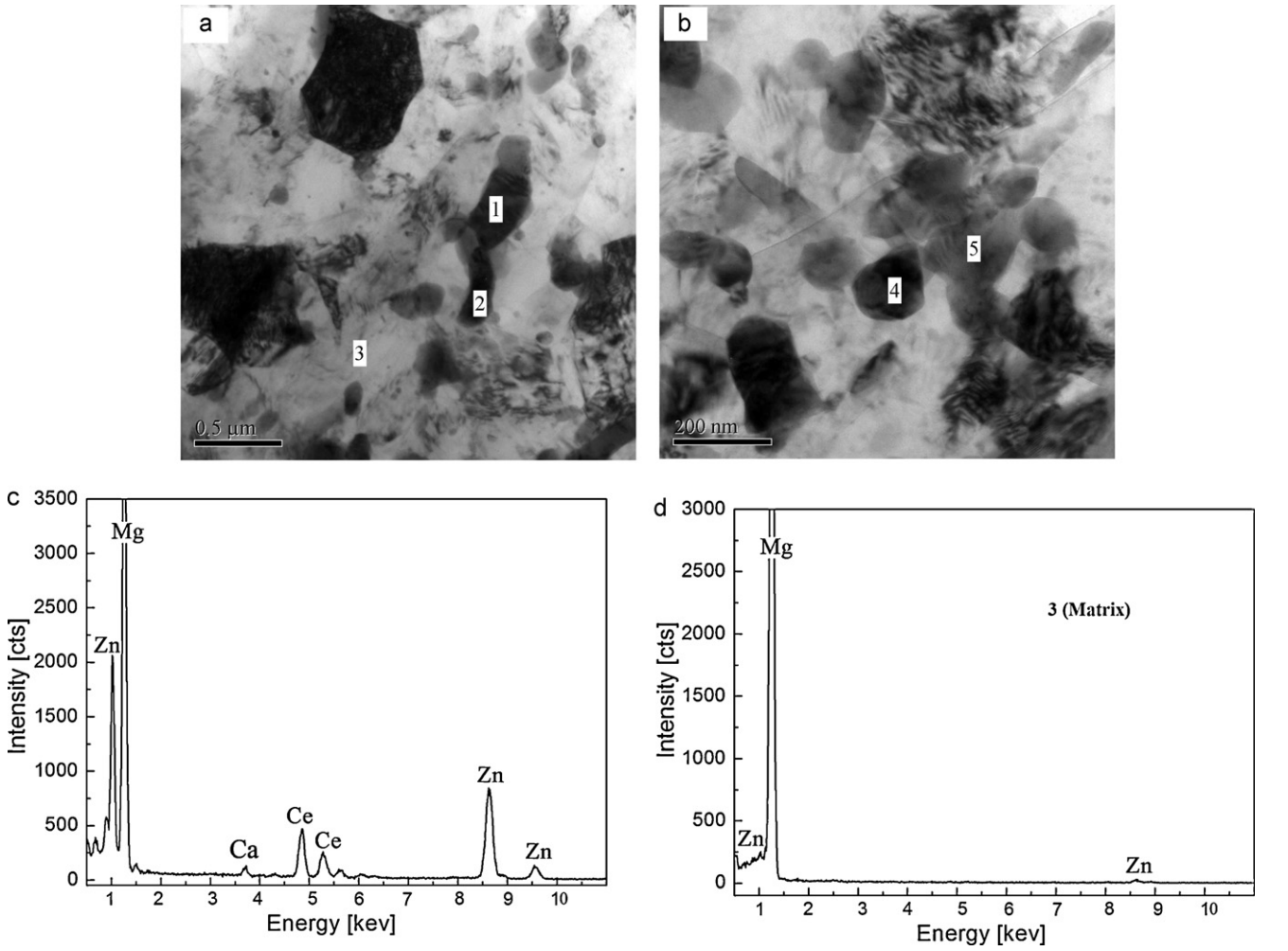

Fig. 5. TEM images of many precipitates with different morphologies around the grain boundary: (a) and (b) the images of the precipitates; (c) EDS results of the precipitates; (d) EDS result of the matrix (marked as 3).

Table 1
The corresponding chemical compositions of the different positions in Fig. 5 analyzed by EDS.

Positions	Elements	Weight percentage (wt.%)	Atomic percentage (at.%)
1	MgK	40.4	72.2
	CeL	34.6	10.7
	ZnK	23.9	15.9
	CaK	1.0	1.1
	Total	100.0	100.0
2	MgK	46.30	76.4
	CeL	30.3	8.7
	ZnK	22.3	13.7
	CaK	1.2	1.2
	Total	100.0	100.0
3	MgK	98.9	99.6
	ZnK	1.1	0.4
	Total	100.0	100.0
4	MgK	50.8	79.7
	CeL	28.3	7.7
	ZnK	19.9	11.6
	CaK	1.1	1.0
	Total	100.0	100.0
5	MgK	58.4	84.1
	CeL	23.5	5.9
	ZnK	17.2	9.2
	CaK	1.0	0.9
	Total	100.0	100.0

mation temperature of T phase in the Mg–10MM–5Zn alloy and that of $Mg_xZn_yCe_z$ phase in the RS/PM Mg–6Zn–5Ce alloy [22]. Therefore, it can be confirmed that in the RS/PM Mg–6Zn–5Ce–1.5Ca alloy the endothermic peak is corresponding to the melting of the $Mg_xZn_yCe_z$ phase with a few Ca (about 1 at.%) and the unknown diffraction peaks in XRD are the $Mg_xZn_yCe_z$ phases with a few Ca (about 1 at.%), in which the atomic percentage ratio of Zn to Ce around the grain boundary is close to 1.5, which is different from the results of literatures [20,21,28]. It has been reported that the Ca-containing ZE41 alloys have Mg_7Zn_3–(RE)–(Ca) eutectic phase, in which Ca is distributed inhomogeneously owing to its strong segregation power, which suggests that the eutectic phase may be formed by the dissolving of RE and Ca in Mg_7Zn_3 phase. However, due to the much higher content of RE in the RS/PM Mg–6Zn–5Ce alloy than that of the ZE41 casting alloy, the stable intermetallic compound $Mg_xZn_yCe_z$ phase can be formed [22]. Therefore, it can be inferred that the formation of $Mg_xZn_yCe_z$ phase with a few Ca (about 1 at.%) in the RS/PM Mg–6Zn–5Ce–1.5Ca alloy may be due to the dissolving of Ca in $Mg_xZn_yCe_z$ phase according to the results of the TEM/EDS (Figs. 4 and 5), so it can be shortened as $Mg_xZn_yCe_z$–(Ca) phase.

In addition, the melting point of the $Mg_xZn_yCe_z$–(Ca) phase in the RS/PM Mg–6Zn–5Ce–1.5Ca alloy (Fig. 2) is a little higher (about 5 °C) than that of the $Mg_xZn_yCe_z$ phase in the RS/PM Mg–6Zn–5Ce alloy [22]. It has been reported that a small quantity of calcium addition to the AZ91 alloy does not result in the formation of a

new phase, but mainly dissolves in the β phase, contributing to the enhanced melting point of the phase [29]. Thus, the dissolving of Ca in the $Mg_xZn_yCe_z$ phase may be the main reason for the increase of the melting point of it.

5. Conclusions

In the present work, the microstructures and phase compositions of the RS/PM Mg–6Zn–5Ce–1.5Ca alloy have been investigated. The results showed that the alloy was characteristics of very fine grains with the size ranging from 200 to 650 nm and was composed of α-Mg, $Mg_xZn_yCe_z$ phase with a few Ca (about 1 at.%) shortened as the $Mg_xZn_yCe_z$–(Ca) phase, and a small quantity of $Mg_{51}Zn_{20}$ phases. The melting point of the $Mg_xZn_yCe_z$–(Ca) phase in the alloy was a little higher than that of the $Mg_xZn_yCe_z$ phase in RS/PM Mg–6Zn–5Ce alloy, which may be due to the dissolving of Ca in it. Moreover, the atomic percentage ratio of Zn to Ce in the $Mg_xZn_yCe_z$–(Ca) phase around the grain boundary was close to 1.5.

Acknowledgements

This work was supported by the Natural Science Foundation Project of CQ CSTC (Grant No. 2010BB4307), Foundation of Chongqing University of Technology in China (Grant No. 2009ZD26) and Youth Foundation Program of Chongqing University of Technology in China (Grant No. 2010ZQ30).

References

[1] Z.L. Liu, W.J. Ding, G.Y. Yuan, Y.P. Zhu, Materials for Mechanical Engineering 25 (2001) 1–4.
[2] G.Q. Liu, L.P. Chen, Y.L. Ai, Special Casting and Nonferrous Alloys 25 (2005) 496–498.
[3] Z.S. Ji, D.F. Li, R.B. Sun, Light Alloy Fabrication Technology 29 (2001) 1–4.
[4] S.M. Masoudpanah, R. Mahmudi, Materials Science and Engineering A 526 (2009) 22–30.
[5] X.Q. Chen, J.W. Liu, C.P. Luo, Materials Review 22 (2008) 58–62.
[6] J.F. Nie, B.C. Muddle, Scripta Materialia 37 (1997) 1457–1481.
[7] B.L. Mordike, W. Riehemann, Key Engineering Materials 97–98 (1994) 13–28.
[8] H. Somekawa, A. Singh, T. Mukai, Scripta Materialia 56 (2007) 1091–1094.
[9] J.Y. Lee, H.K. Lim, D.H. Kim, W.T. Kim, D.H. Kim, Materials Science and Engineering A 448–451 (2007) 987–990.
[10] F. Petsol′d, B. Beyer, Metal Science and Heat Treatment 13 (1971) 369–371.
[11] M.E. Drits, E.M. Padezhnova, N.V. Miklina, Russian Metallurgy 1 (1971) 143–146.
[12] T.V. Dobatkina, E.V. Muratova, I.I. Drozdova, Russian Metallurgy 1 (1987) 205–208.
[13] M.E. Drits, E.I. Drozdova, I.G. Korol′kova, V.V. Kinzhibalo, A.T. Tyvanchuk, Russian Metallurgy 2 (1989) 195–197.
[14] L.Y. Wei, G.L. Dunlop, H. Westengen, Metallurgical and Materials Transactions A 26 (1995) 1947–1955.
[15] J. Yang, J. Wang, L. We Xiao, L.D. Wang, Y.M. Wu, H.J. Zhang, L.M. Wang, Materials Science Forum 561–565 (2007) 199–202.
[16] Y.L. Tang, D.S. Zhao, Z.P. Luo, N.F. Shen, S.Q. Zhang, Scripta Metallurgica et Materialia 29 (1993) 955–958.
[17] Z.P. Luo, S.Q. Zhang, Y.L. Tang, D.S. Zhao, Scripta Metallurgica et Materialia 32 (1995) 1411–1416.
[18] I.A. Anyanwu, Y. Gokan, A. Suzuki, S. Kamado, Y. Kojima, S. Takeda, T. Ishida, Materials Science and Engineering A 380 (2004) 93–99.
[19] G.H. Wu, Y. Fan, H.T. Gao, C.Q. Zhai, Y.P. Zhu, Materials Science and Engineering A 408 (2005) 255–263.
[20] J.H Jun, B.K. Park, J.M. Kim, K.T. Kim, W.J. Jung, Materials Science Forum 510–511 (2006) 214–217.
[21] M. Zhu, S.Y. Sun, W.B. Gui, Jiangsu Metallurgy 30 (2002) 1–5.
[22] T. Zhou, Research on Microstructures and Properties of Rapidly Solidified Mg–Zn Based Magnesium Alloy, Hunan University, Changsha, 2009, pp. 106–108.
[23] C.J. Xu, X.F. Guo, Z.M. Zhang, S.Z. Jia, L. Liu, Ordnance Material Science and Engineering 29 (2006) 9–12.
[24] Y. Wu, T.J. Piccone, Y. Shiohara, M.C. Flemings, Metallurgical and Materials Transactions A 18 (1987) 915–924.
[25] T.J. Piccone, Y. Wu, Y. Shiohara, M.C. Flemings, Metallurgical and Materials Transactions A 18 (1987) 925–932.
[26] L.Y. Wei, G.L. Dunlop, H. Westengen, Journal of Materials Science 32 (1997) 3335–3340.
[27] L.Y. Wei, G.L. Dunlop, Journal of Materials Science Letters 15 (1996) 4–7.
[28] T. Itoi, Y. Yano, S. Fudetani, Y. Kawamura, M. Hirohashi, Journal of Japan Institute of Light Metals 56 (2006) 543–549.
[29] W.W. Du, Y.S. Sun, X.G. Min, F. Xue, M. Zhu, D.Y. Wu, Materials Science and Engineering A 356 (2003) 1–7.